Improved positioning and detectability of microparticles in droplet microfluidics using two-dimensional acoustophoresis

M Ohlin[1] , **A Fornell**[2] , **H Bruus**[3] and **M Tenje**[1,2,4]

[1] Department of Engineering Sciences, Uppsala University, Uppsala, Sweden
[2] Department of Biomedical Engineering, Lund University, Lund, Sweden
[3] Department of Physics, Technical University of Denmark, Kgs. Lyngby, Denmark
[4] Science for Life Laboratory, Uppsala University, Uppsala, Sweden

E-mail: mathias.ohlin@angstrom.uu.se

Abstract

We have fabricated a silicon-glass two-phase droplet microfluidic system capable of generating sub 100 μm-sized, $\varnothing = (74 \pm 2)$ μm, spherical droplets at rates of up to hundreds of hertz. By implementing a two-dimensional (2D) acoustophoresis particle-positioning method, we show a fourfold improvement in both vertical and lateral particle positioning inside the droplets compared to unactuated operation. The efficiency of the system has been optimized by incorporating aluminum matching layers in the transducer design permitting biocompatible operational temperatures (<37 °C). Furthermore, by using acoustic actuation, $(99.8 \pm 0.4)\%$ of all encapsulated microparticles can be detected compared to only $(79.0 \pm 5.1)\%$ for unactuated operation. In our experiments we observed a strong ordering of the microparticles in distinct patterns within the droplet when using 2D acoustophoresis; to explain the origin of these patterns we simulated numerically the fluid flow inside the droplets and compared with the experimental findings.

S Supplementary material for this article is available online

(Some figures may appear in colour only in the online journal)

1. Introduction

Droplet microfluidics which has emerged from microfluidics, a well-established research field [1] almost three decades old, has of recent years expanded rapidly and offers now solutions to a vast amount of biotechnological problems [2, 3]. Two-phase droplet microfluidic systems are typically used to compartmentalize assays in nanoliter or less aqueous droplets surrounded by an immiscible carrier fluid. These, often water-in-oil, self-contained and dispersed microreactors provide increased throughputs, reduced consumption and costs of reagents and samples due to the very small droplet volumes, which facilitates, e.g. single-cell analysis [2, 4, 5]. Moreover, droplet microfluidics has the ability to be automated and

parallelized, drastically decreasing the experiment time compared to assays in normally much larger reaction volumes. Droplet microfluidics provide a broad spectrum of complex assays and reactions, for example, droplet microfluidics has been used for high-throughput biological assays such as detection and analysis of cell-surface protein biomarkers, directed evolution of yeast cells, and encapsulation and screening of single-cells [6–9]. Importantly, all of these assays require encapsulation of microparticles such as cells or microbeads, and they all utilize optical detection methods.

Optical read-out is commonly used in combination with droplet microfluidics as a direct read-out method or internal trigger for consecutive steps in a microfluidic circuit [10–12]. To be able to easily detect the encapsulated microparticles

optically, it is crucial that they are in focus, i.e. within the depth-of-field (DOF) of the optical imaging system. This is especially true for high numerical aperture (NA) objectives with their short DOF [13], often much shorter than the microfluidic channel depth. Although optical detection is one of the most versatile read-out methods [14], there are still many challenges as a result of sedimentation and unpredictable positioning of the encapsulated microparticles inside the droplets.

In this paper, we present a method to position microparticles at optically ideal positions inside the droplets both laterally and vertically using acoustic standing waves. Acoustic standing wave manipulation techniques in continuous flow microfluidics termed acoustophoresis offers a gentle non-contact, label-free, charge independent, and in-chip particle and cell handling method [15]. There are two main types of acoustophoresis both defined by how the sound is propagated through the system, bulk acoustic waves (BAW) acoustophoresis where the sound is propagated through the bulk of the material and surface acoustic waves (SAW) acoustophoresis where the sound propagates along the surface of the material. Both types of acoustophoresis have been used to manipulate suspended microparticles [16, 17] and droplets [18, 19]. Rather than using channel geometries to restrict the droplet movement confining the droplet into the DOF [6] we have instead focused on contact-less acoustophoretic manipulation of the suspended microparticles prior to droplet encapsulation, leaving the droplet undisturbed. We have previously reported on lateral positioning of microparticles inside large droplets ('plugs') by one-dimensional (1D) BAW acoustophoresis [20], and in this paper we expand the droplet microfluidic toolbox with two-dimensional (2D) BAW acoustophoresis [21–23] prior to droplet encapsulation in a purpose build silicon-glass droplet microfluidic system optimized for BAW to obtain improved microparticle positioning and detectability within the droplets.

2. Theory

Acoustophoresis is a non-contact method to manipulate microparticles in microfluidic channels using ultrasonic standing waves. The primary acoustic radiation force focuses microparticles to either the pressure nodal lines or anti-nodal lines depending on the acoustic properties of the microparticles in relation to that of the surrounding fluid [24]. Polystyrene microparticles and cells in water have a positive acoustic contrast factor and are therefore focused to the pressure nodal lines. Acoustophoresis can be applied in either one or two dimensions [21, 23]. Acoustic microparticle manipulation in a water-filled rectangular microfluidic channel of height H and width W at the half-wave resonances is shown schematically in figure 1. In figure 1(a) an acoustic vertical standing half-wave with frequency f_1 is created in the channel by setting $f_1 = 2c_0/H$, where c_0 is the speed of sound in water. This wave causes microparticles with a positive acoustic contrast factor to be focused in the horizontal xy-plane located in the middle of the channel, and further it counteracts sedimentation. As shown in figure 1(b), microparticles can also be focused in the vertical xz-plane by applying an acoustic horizontal standing half-wave at frequency $f_2 = 2\,c_0/W$. This wave causes

microparticles with a positive acoustic contrast factor to be focused in the vertical xz-plane in the middle of the channel. Figure 1(c) shows that when frequency f_1 and f_2 are applied simultaneously, a 2D acoustic standing wave results. This wave causes microparticles with a positive acoustic contrast factor to be focused at the intersection of the horizontal and vertical plane in the middle of the channel, a situation termed 2D acoustophoresis. When a Poiseuille flow is set up along the channel x-axis, focusing by 2D acoustophoresis ensures that all microparticles experience the same velocity in the flow profile (see the red region in figure 1).

For two-phase flow, where a water droplet is submerged in oil flowing through a rectangular channel, intra-droplet flow rolls develop driven by the viscous forces between the water and oil phases at the droplet surface [25]. In a narrow channel, the flow field is toroidal with a significant horizontal component, while in a wide channel mainly vertically oriented flow rolls appear as shown in section 4. This flow pattern governs the intra-droplet microparticle dynamics after the formation of the droplets.

3. Experimental

3.1. Fabrication of the silicon-glass chip

An overview of the system implementing dual transducer technology for 2D acoustophoresis is shown in figure 2, a photograph showing the system during operation can be seen in the supplementary material (figure S1) (stacks.iop.org/JMM/27/084002/mmedia). The system consists of a silicon-glass chip fabricated in-house using photolithography and dry-etching technology. The channels and droplet generator structures are dry-etched in a $\langle 1\ 0\ 0 \rangle$ oriented, 500 μm thick silicon wafer using deep reactive ion etching (DRIE) producing approximately 100 μm deep channels with vertical side walls. The smallest features of the flow-focusing droplet generator are the 50 μm wide inlets and outlets which were analyzed by scanning-electron-microscope (SEM). Inlets and outlet were manually drilled through the silicon wafer using a micro diamond-drill bit (400 μm in diameter) attached to a Dremel rotary power tool. To seal the system, anodic bonding of a 700 μm thick borofloat-33 glass wafer to the silicon wafer was performed (see 'glass' in figure 2(b)). The bonded silicon and glass wafers were diced into individual chips using a diamond dicing saw. Connectors made of 10 mm long silicone tubing (228-0700, VWR, Sweden) with an inner diameter of 1 mm were glued (Wacker RTV-1 A07, Wacker Chemie AG, Germany) on the silicon backside to the drilled inlets and outlet. Prior to usage the channels were treated with a surface coating agent (Repel-silane ES, GE Healthcare, USA) to render the channels hydrophobic for increased droplet formation stability.

3.2. Transducer design

In the acoustic active region of our system, the channel has height $H = 98$ μm and width $W = 150$ μm. For water, this results in the respective half-wave resonance frequencies $f_1 = 7.7$ MHz and $f_2 = 5.0$ MHz. To obtain 2D acoustophoresis
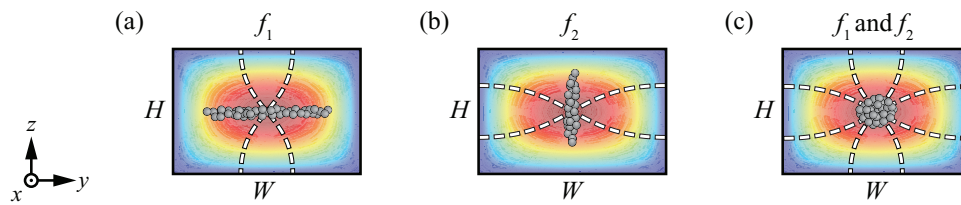
Figure 1. Schematic cross-section of a water-filled rectangular channel showing the working principle of 1D and 2D acoustophoresis, as microparticles experience the half-wave frequencies (a) f_1 (1D vertical acoustophoresis), (b) f_2 (1D horizontal acoustophoresis), and (c) f_1 and f_2 combined (2D acoustophoresis). The color plot represents the Poiseuille flow velocity profile from zero velocity (blue) to maximum velocity (red).
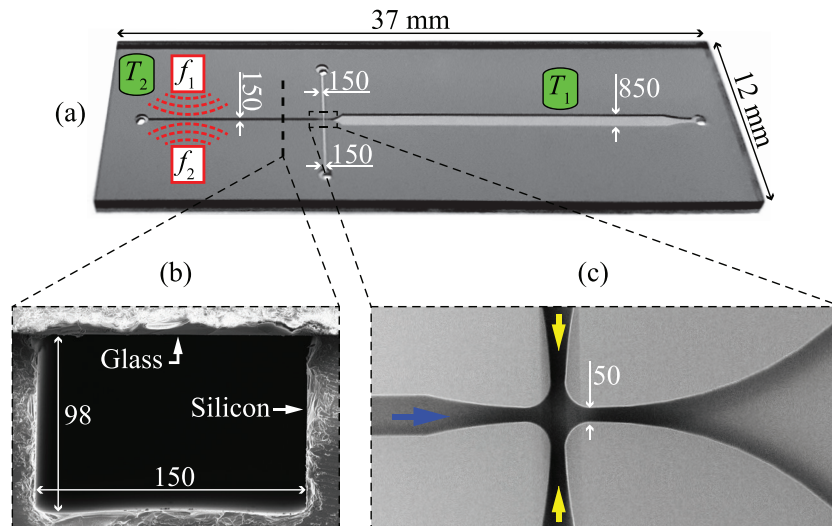

Figure 2. (a) A photograph of the silicon-glass chip with overlaid schematics. The unit is μm if not indicated otherwise. Here f_1, f_2 and T_1, T_2 are the locations of the transducers and thermocouples attached to the silicon backside, respectively. (b) SEM image showing the cross-section of the inlet channel carrying the dispersed water phase. (c) SEM image of the flow-focusing droplet generator. Here, the fluid flow directions are indicated for the continuous oil phase (yellow arrows) and dispersed water phase (blue arrow).

at these frequencies, a dual transducer technology was implemented by the use of two piezoelectric elements with thicknesses of 0.25 mm (APC-840, APC International, Ltd, USA) having a resonance frequency of 8 MHz and 0.4 mm (APC-841, APC International, Ltd, USA) having a resonance frequency of 5 MHz. Both piezoelectric elements were fitted with optimized matching and backing layers. The matching layers were made of Aluminum-7075, since with its given density ρ and sound speed c, it has an acoustic impedance $Z = \rho c$, which is a close match to the theoretical optimum value Z_{opt} given as the geometric mean of the acoustic impedances of the piezoelectric material (pz) and of silicon (si), $Z_{opt} = \sqrt{Z_{pz}Z_{si}}$ [26]. Furthermore, the layer thicknesses are chosen to ensure maximum transmission for plane waves. Using the expressions in Ref. [18], we find the optimal matching layer thicknesses for Aluminum-7075 to be 2.57 mm at 8 MHz and 2.84 mm at 5 MHz, resulting in theoretical transmission coefficients around 94%. The aluminum matching layers were attached with a thin layer of cyanoacrylate adhesive (Loctite 420, Henkel Norden AB, Sweden) to the piezoelectric elements. Electrical connectors where attached using solder and small 26 AWG enameled copper wires to minimize mass loading effect such as resonance frequency shifts. A high bond strength epoxy adhesive (Loctite 3450, Henkel Norden AB, Sweden) was dispensed on the backside of the piezoelectric elements working as backing

layers. As a result of adding backing and matching layer, the electrical resonance frequency of the transducers broadens, enabling efficient frequency-modulation (FM) actuation of the transducers and resulting in a more robust 2D acoustophoresis [27, 28]. Additionally, using FM it is possible to compensate for the small variations in channel geometry caused by the dry-etching technique: an FM with 100 kHz span and a rate of 1 kHz results in a depth-compensation ability of approximately ±3 μm. Additionally, using FM actuation the system becomes less sensitive to resonance drifts due to temperature changes. Finally, the use of aluminum as a matching layer material ensures good heat transporting capabilities [29].

3.3. Materials and instrumentation

The flow-focusing droplet generator is designed to suspend microparticles in water droplets surrounded by immiscible oil. In this system the continuous oil phase consisted of fluorinated oil Novec HFE-7500 (Kemi-Intressen AB, Sweden) with 2% Krytox (The Chemours Company, USA) surfactant. The dispersed water phase consisted of Milli-Q water with 0.1% Triton-X (X100, DuPont, USA) surfactant, containing suspended 9.9 μm-diameter polystyrene microparticles (Fluoro-Max G1000, Thermo Scientific, USA) at a concentration of 2.3×10^6 particles ml^{-1}. Both the surfactants Triton-X
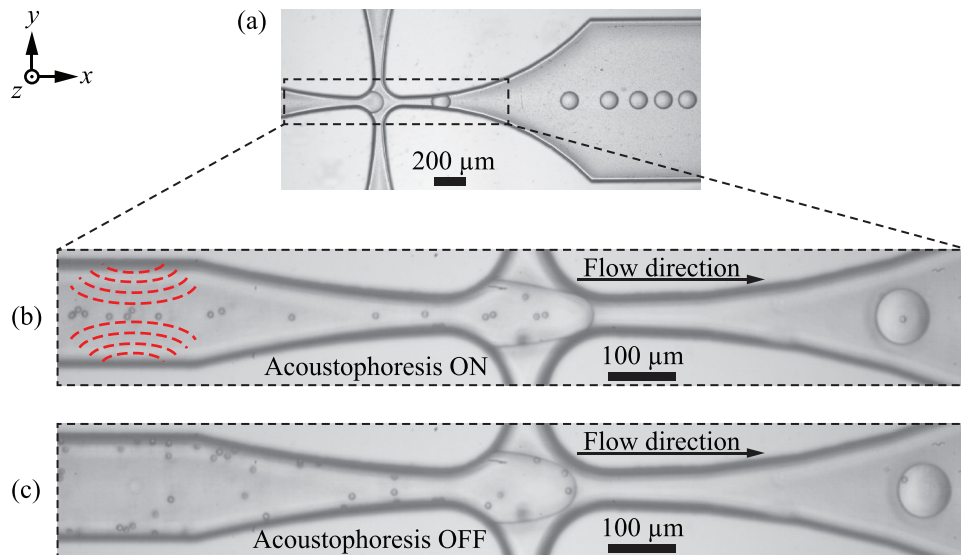
Figure 3. (a) Photograph showing the droplet formation process. Inserts are zoomed still frames from the high-speed video showing how the microparticles are aligned during the droplet formation processes when the 2D acoustophoresis is (b) on, and (c) off.

and Krytox were used to stabilize the interface and prevent coalescence of the water-in-oil droplets [30]. Moreover, Triton-X in the dispersed water phase helps to prevent particle agglomeration by increasing the hydrophilicity of the polystyrene microparticles facilitating single-particle encapsulation. The two piezoelectric transducers were driven by a two-channel function generator (AFG3022C, Tektronix, USA) generating frequency modulated, sinusoidal 10 V_{pp} (peak-to-peak voltage) signals enabling 2D acoustophoresis. The chip was connected to a syringe pump (Nemesys, Cetoni GmbH, Germany) equipped with plastic syringes using polyethylene tubing (427406, Becton Dickinson and Company, USA) with an outer diameter of 1.09 mm resulting in a tight fit with the glued inlet and outlet silicone connectors. The continuous oil phase was pushed into the two inlets (see the yellow arrows in figure 2(c)) at a flow rate of 40 μl min^{-1} per inlet, whereas the dispersed water phase was pulled, to minimize microparticle sedimentation in the syringe, with a flow rate of 5 μl min^{-1}. A high-speed camera (Miro M310, Vision Research Inc., USA) mounted to an inverted microscope (TE2000-U, Nikon, Japan) was used with a 10×/0.30 Plan Fluor objective (Nikon, Japan) with a DOF <15 μm to record high-speed videos with a frame rate of 2000 frames s^{-1}. Using the internal microscope magnification of 1.5× the total magnification was 15×. To ensure adequate lighting an 80 W LED (pE-300 white, CoolLED Ltd, UK) was used in full white intensity mode. To minimize heating due to electrical losses in the piezoelectric material of the two transducers, a 12 Vdc blower (GB1205PKV1-8AY, Sunonwealth Electric Machine Industry Co., Ltd, Taiwan) was implemented and used continuously during the experiments. The temperature on the chip (see T_1 and T_2 in figure 2(a)) was monitored using two K-type isolated junction surface temperature thermocouple probes (433–4313, RS Components Ltd, UK) attached with heat conducting adhesive (WLK 10, Fischer Elektronik GmbH & Co. KG, Germany), and the room temperature was measured using a single K-type exposed junction thermocouple probe

(363-0250, RS Components Ltd, UK); all three connected to a four channel data logger (TM-947SD, Lutron Electronic Enterprise CO., Ltd, Taiwan).

3.4. Image analysis

The acquired high-speed videos were converted into still frames using the camera software. The still frames were manually analyzed in ImageJ [31] to estimate droplet size, droplet generation frequency as well as quantity and detectability of the encapsulated microparticles. MATLAB (R2015b, The MathWorks Inc., USA) was used to manually determine positions of individual single encapsulated microparticles within each droplet by marking positions and calculating distances from droplet center.

3.5. Theoretical simulations

Numerical simulations were carried out using COMSOL Multiphysics 5.2 (COMSOL AB, Sweden). We studied segments of the rectangular channel of length $L = 360$ μm, height $H = 98$ μm, and varying width W. First, we studied the acoustophoretic force F_{ac} on 10 μm-diameter spherical polystyrene microparticles in a water-filled channel of width $W = 150$ μm and having acoustically hard walls. Using the methods of Ref. [32] extended from 2D to 3D, we found that oscillating the top-bottom walls at 7.7 MHz and the side walls at 5.0 MHz with an amplitude of 0.1 nm, the expected half-wave resonances were found, and F_{ac} was calculated to be around 0.1 nN ensuring good 2D acoustophoretic focusing. Then, keeping the two frequencies and the channel geometry fixed, but changing the liquid to HFE-7500 oil and embedding a 74 μm-diameter water droplet at the center of the channel segment, we found that the acoustic resonances disappeared and F_{ac} dropped three orders of magnitude to around 1 pN, thus rendering acoustophoresis negligible. Similar results for water droplets in oil were obtained in subsequent simulations
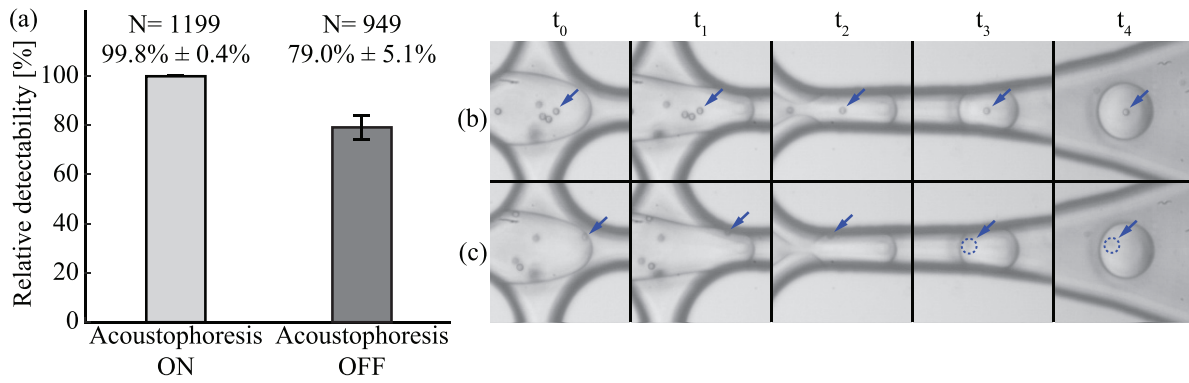
Figure 4. (a) Relative particle detectability with and without 2D acoustic actuation of the microparticles in the inlet channel. (b) and (c) zoomed still frames from the high-speed video showing encapsulation of a microparticle when the 2D acoustophoresis is (b) on and (c) off. The encapsulated microparticle in (b) can easily be detected optically whereas the encapsulated microparticle in (c) is out of focus.

for a more narrow channel with $W = 85$ μm and a wider channel with $W = 200$ μm.

We then moved on to simulate the velocity field as an incompressible Stokes flow inside a spherical 74 μm-diameter water droplet submerged in HFE-7500 oil that flows through the channel. We studied this both for a narrow width $W = 85$ μm and for a wide one $W = 200$ μm. Since a relative flow velocity as low as $v = 20$ mm s^{-1} around a sphere of diameter $d = 74$ μm leads to a Stokes drag force of $F_{\text{drag}} = 3\pi\eta dv \approx 1$ nN, the minute 1 pN-acoustophoretic force is neglected. We imposed the Poiseuille flow profile at the rectangular inlet and outlet [33], we used the no slip condition at the channel walls, and on the droplet surface in its rest frame, we applied zero normal velocity and continuous tangential stress. By iteration, we adjusted the amplitude of the Poiseuille flow such that the droplet center speed was 110 mm s^{-1} relative to the fixed walls as in the experiments, while the surface integral of the stress on the droplet surface was zero (the stationary situation).

Finally, using the COMSOL particle trajectory module, we studied the motion of spherical 10 μm-diameter polystyrene tracer particles inside the droplet for the obtained velocity fields [32]. While acoustophoresis is negligible for the particle dynamics in the droplet, it enters through the initial position of the tracer particles: with acoustic actuation, the tracer particles start out near the intersection of the two focal planes, while without the acoustic actuation, they start out randomly distributed throughout the droplet volume.

4. Results and discussion

The temperature of the system with blower assisted cooling measured with the thermocouples T_1 and T_2 were (28.6 ± 0.5) °C and (29.2 ± 0.5) °C, respectively, at a room temperature of (24.2 ± 0.5) °C and actuation voltages of 10 V$_{\text{pp}}$ for each transducer. Owing to relatively high thermal conductivity of silicon, the temperature gradient across the system is negligible. The sub-30 °C operational temperatures, which is beneficial for biological samples such as cells [34], can partly be attributed to the aluminum matching layers which physically elevate the heat generating piezoelectric elements away from the chip surface and at the same time functions as heat sinks.
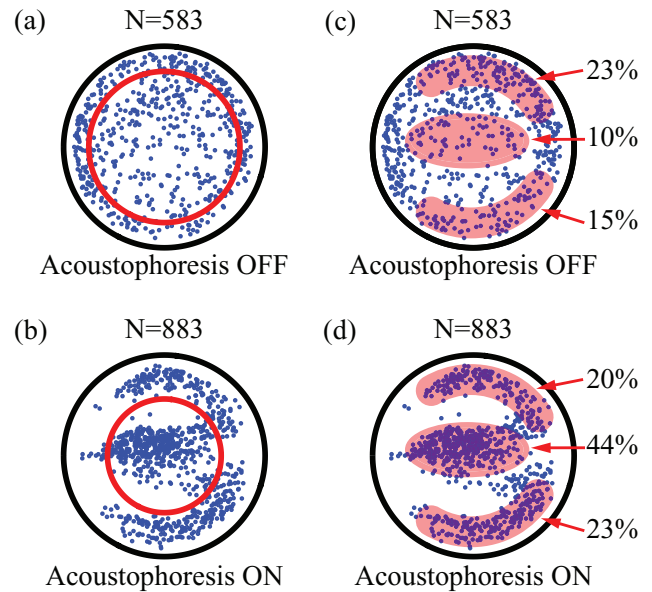

Figure 5. The positions (blue dots) of a total of 1466 single encapsulated microparticles are superimposed within a single droplet moving to the right. (a) and (b) the red circle indicates the median particle distance from the droplet center. (c) and (d) three regions with high particle concentration are marked.

Figure 3 shows the formation of water droplets in the oil phase, and the effect of 2D acoustophoresis in the inlet channel. The system can produce droplets as small as (74 ± 2) μm in diameter resulting in droplet volumes in the order of hundreds of picoliter. With the acoustic actuation on, the suspended microparticles are focused by 2D acoustophoresis along the channel center axis in the water phase, before entering the droplet formation region. The system can be driven with a droplet generation frequency of (298 ± 85) Hz with retained 2D acoustophoretic function, see figure 3(b). For the unactuated control experiments, microparticles enter the flow-focusing junction randomly, see figure 3(c).

A comparison of the relative particle detectability between the acoustic-actuated and the unactuated operation of the system can be seen in figure 4 using data from four sets of experiments. The recorded 40 000 still images were manually analyzed, and among these a total of 2148 droplets containing microparticles were identified, while empty droplets
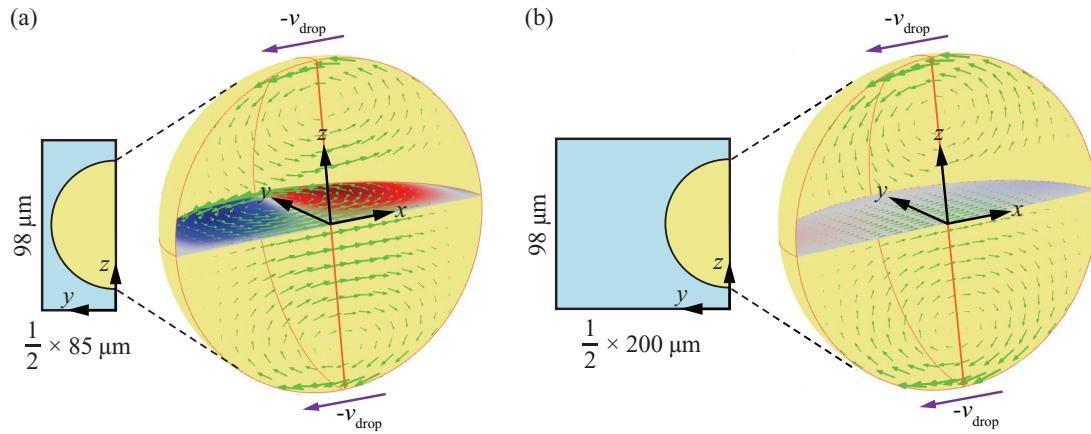
Figure 6. Numerical simulations of the velocity field in the rest frame of a spherical 74 μm-diameter water droplet submerged in HFE-7500 oil that flows through a rectangular channel of height $H = 98$ μm and width W. The droplet center moves along the x-axis with the speed $v_{drop} = 110$ mm s^{-1} (purple arrows) relative to the fixed walls. Due to mirror symmetry around the vertical xz center plane only one half of the droplet is shown. The velocity (green arrows) relative to the droplet center are shown in the vertical xz center plane and in the horizontal xy center plane for (a) a narrow channel $W = 85$ μm, and (b) a wide channel $W = 200$ μm. The color plot in the xy-plane represents the y-component of the velocity field from -25 mm s^{-1} (blue), through 0 mm s^{-1} (gray), to 25 mm s^{-1} (red). The insets show the vertical cross section of the channel with oil (light blue) at the center position of the droplet (beige).
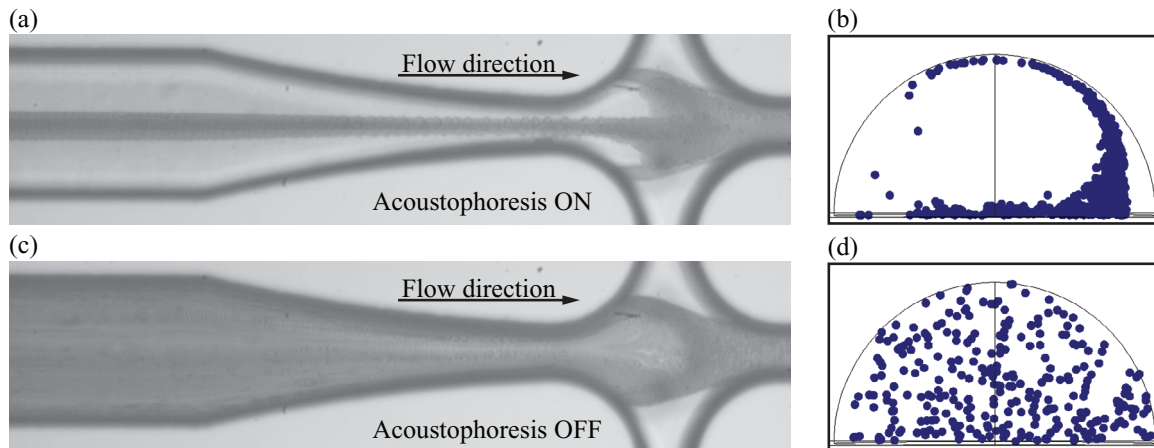

Figure 7. (a) Minimum intensity z-projection to the xy-plane of the particle distribution with 2D acoustophoresis during the formation of 865 droplets. (b) Numerical simulation of 800 particles inside a droplet advected by the internal fluid flow of figure 6(a), and with initial particle positions taken to be near the horizontal center axis of the droplet due to 2D acoustophoresis. (c) Minimum intensity z-projection to the xy-plane showing particle distribution for the formation of 521 droplets without 2D acoustophoresis. (d) Same as panel (b), but with the initial particle positions taken to be evenly distributed throughout the droplet.

were excluded. For each particle-containing droplet the relative detectability was determined. The distinction between a detected and an undetected microparticle is shown in examples in figures 4(b)–(c). The effect of 2D acoustophoresis is two-fold; it prevents sedimentation, and it moves particles towards the channel center thus minimizing particle-wall interactions. These acoustophoretic effects combined lead to a nearly 100% relative detectability of the encapsulated microparticles, as opposed to only 79% without acoustophoresis.

Figure 5 shows particle positions for the two operational modes of the system: 2D acoustophoresis on and off. The positions are acquired approximately 500 μm after the flow-focusing junction inside the droplets which travel with a speed of (110 ± 13) mm s^{-1}. For each droplet containing a single microparticle, the position was manually determined and superimposed. The result of 2D acoustophoresis on particle position (blue dots) is depicted in two ways: figures 5(a) and

(b) show the median distance (red circle) from the droplet center, while (c) and (d) show the positions divided into three regions. It is clearly seen that 2D acoustophoresis positions microparticles closer to the droplet center and that the majority of the encapsulated microparticles ends up in the central region compared to the unactuated operation of the system. Using 2D acoustophoresis, 86% of the microparticles are focused to one of the three regions within the droplet, in contrast to only 48% for the unactuated control. In particular, with 2D acoustophoresis the central region holds 44% of all microparticles compared to only 10% for the unactuated control. This fourfold increase of microparticles located in the center part of the droplet using 2D acoustophoresis is favorable for all biological droplet assays where single-particle analysis with minimal optical aberration is of importance. Interestingly, with 2D acoustophoresis the particle positions are distributed in three distinct regions as seen in figure 5(d).

The experimental findings can be explained qualitatively by numerical studies of the flow field inside a given droplet. Immediately following the droplet formation, the droplet moves along a narrow channel segment with a height of 98 μm and a width of only 50 μm. The droplet center moves with the speed $v_{drop} = 110$ mm s^{-1} relative to the fixed confining walls, and this results in a toroidal flow field inside the droplet due to the viscous shear forces, as shown numerically in figure 6(a). In the simulations, where the channel width has been increased to 85 μm to avoid deformation of the droplet, the toroidal flow field shows up as distinct pairs of counter-rotating vortices in both the horizontal and vertical center planes. The significant *y*-component of the flow field in the horizontal center plane is emphasized in the color plot (dark blue and dark red colors). Then, 200 μm downstream, the channel begins to widen, and ultimately it reaches a width of 850 μm. This situation we simulated using a width of only 200 μm to reduce the very demanding computer-memory requirements of the 3D simulations. However, already at this width, the vertical walls are so far from the droplet that the much nearer horizontal walls completely dominates the flow field inside the droplet. This is seen in figure 6(b) by the strong flow rolls that remain in the vertical center plane, while the *y*-component of the flow field nearly vanishes in the *xy*-plane (grayish color).

These flow fields combined with the initial position of the particles at the location of the droplet formation can explain the observations. Clearly, using 2D acoustophoresis the suspended microparticles in the water phase are focused both horizontally and vertically in the middle of the inlet channel, see figures 3(b), 4(b) and 7(a). This effect is partially preserved at the location of the droplet formation as shown in figure 7(a), where a projection onto the *xy*-plane of approximately 5000 still frames is displayed. In the corresponding simulation we therefore take the initial particle positions to be distributed close to the center axis, and then let it propagate in time using the flow field of figure 6(a). Due to the particle-wall interactions in the 98 μm-high channel, the Stokes drag coefficient of the 10 μm-diameter particles is enhanced by a factor of 1.11 according to the Faxén–Brenner expression given in [35]. The result after 1.5 ms, shown in figure 7(b), indicates that particles encapsulated close to the droplet center will be moved by the horizontal part of the toroidal flow field and therefore be spread out along the *x*-axis and the droplet periphery much like the experimental results in figure 5(d). Without the acoustic actuation, we observe that the microparticles arrive to the droplet formation location at random positions, and then they are advected by the toroidal flow field to end up anywhere in the entire droplet volume (see figure 7(c)). In the corresponding simulation we therefore take the initial particle positions to be distributed evenly throughout the droplet volume. We then again simulate the propagation for 1.5 ms using the flow field of figure 6(a), and the resulting distribution, shown in figure 7(d), indicates that now the particles end up with randomly distributed positions in agreement with the observations in figure 5(c). For a deeper analysis of the internal fluid flows inside moving droplets of various sizes and channel geometries the authors refer to the work [36–38], where micro-particle image velocimetry was used for fluid flow analysis within droplets. However, the patterns shown in figure 5 are dependent on the time scale of the system, i.e. the time it takes for a droplet to move from the droplet formation location to the imaging point, here approximately 5 ms, as well as on the channel geometry, since both these parameters influence the particle transport and hence the location of the encapsulated microparticles. Furthermore, a lower bound for the particle size used in our acoustophoretic system is the general value of 2 μm, below which acoustic streaming begins to dominate over the acoustic radiation force [32]. An upper bound would be the channel height *H* or width *W,* where particle–wall interactions and clogging effects begin to dominate.

5. Conclusion

In this work, we have presented a silicon-glass two-phase droplet microfluidic system capable of producing sub 100 μm-sized spherical water droplets in oil at a rate of hundreds of droplets per second. We have implemented dual transducer technology for 2D acoustophoresis to avoid particle sedimentation and particle–wall interactions and for improved lateral and vertical particle positioning inside the droplets. To understand the effect 2D acoustophoresis has on the encapsulated microparticles we simulated numerically the fluid flow inside the droplets for various scenarios concluding that the initial particle position at the location of droplet formation is decisive. By equipping the two ultrasonic transducers with optimized aluminum matching layers the system showed biological compatible operation temperatures. As a result of 2D acoustophoresis, the system showed a fourfold increase in the amount of particles located in the central region of the droplet compared to unactuated operation. Moreover, using 2D acoustophoresis close to 100% of all encapsulated microparticles were detected compared to only 79% for unactuated operation of the system. This makes 2D acoustophoresis suitable in droplet-based biological assays in which the encapsulated particles are scarce and a high detectability is paramount such as in single-cell analysis.

Acknowledgments

ORCID

M Ohlin https://orcid.org/0000-0002-7023-4772
A Fornell https://orcid.org/0000-0001-7980-376X
H Bruus https://orcid.org/0000-0001-5827-2939
M Tenje https://orcid.org/0000-0002-1264-1337

References

[1] Sackmann E K, Fulton A L and Beebe D J 2014 The present and future role of microfluidics in biomedical research *Nature* **507** 181–9

[2] Teh S Y, Lin R, Hung L H and Lee A P 2008 Droplet microfluidics *Lab Chip* **8** 198–220

[3] Schneider T, Kreutz J and Chiu D T 2013 The potential impact of droplet microfluidics in biology *Anal. Chem.* **85** 3476–82

[4] Whitesides G M 2006 The origins and the future of microfluidics *Nature* **442** 368–73

[5] Seemann R, Brinkmann M, Pfohl T and Herminghaus S 2012 Droplet based microfluidics *Rep. Prog. Phys.* **75** 016601

[6] Brouzes E *et al* 2009 Droplet microfluidic technology for single-cell high-throughput screening *Proc. Natl Acad. Sci. USA* **106** 14195–200

[7] Clausell-Tormos J *et al* 2008 Droplet-based microfluidic platforms for the encapsulation and screening of Mammalian cells and multicellular organisms *Chem. Biol.* **15** 427–37

[8] Koster S *et al* 2008 Drop-based microfluidic devices for encapsulation of single cells *Lab Chip* **8** 1110–5

[9] Joensson H N *et al* 2009 Detection and analysis of low-abundance cell-surface biomarkers using enzymatic amplification in microfluidic droplets *Angew. Chem. Int. Ed. Engl.* **48** 2518–21

[10] Guo M T, Rotem A, Heyman J A and Weitz D A 2012 Droplet microfluidics for high-throughput biological assays *Lab Chip* **12** 2146–55

[11] Baret J C *et al* 2009 Fluorescence-activated droplet sorting (FADS): efficient microfluidic cell sorting based on enzymatic activity *Lab Chip* **9** 1850–8

[12] Joensson H N and Andersson Svahn H 2012 Droplet microfluidics—a tool for single-cell analysis *Angew. Chem. Int. Ed. Engl.* **51** 12176–92

[13] Wiklund M, Brismar H and Onfelt B 2012 Acoustofluidics 18: microscopy for acoustofluidic micro-devices *Lab Chip* **12** 3221–34

[14] Zhu Y and Fang Q 2013 Analytical detection techniques for droplet microfluidics—a review *Anal. Chim. Acta* **787** 24–35

[15] Lenshof A, Magnusson C and Laurell T 2012 Acoustofluidics 8: applications of acoustophoresis in continuous flow microsystems *Lab Chip* **12** 1210–23

[16] Ding X Y *et al* 2012 Standing surface acoustic wave (SSAW) based multichannel cell sorting *Lab Chip* **12** 4228–31

[17] Petersson F, Aberg L, Sward-Nilsson A M and Laurell T 2007 Free flow acoustophoresis: microfluidic-based mode of particle and cell separation *Anal. Chem.* **79** 5117–23

[18] Leibacher I, Reichert P and Dual J 2015 Microfluidic droplet handling by bulk acoustic wave (BAW) acoustophoresis *Lab Chip* **15** 2896–905

[19] Li S X *et al* 2013 An on-chip, multichannel droplet sorter using standing surface acoustic waves *Anal. Chem.* **85** 5468–74

[20] Fornell A *et al* 2015 Controlled lateral positioning of microparticles inside droplets using acoustophoresis *Anal. Chem.* **87** 10521–6

[21] Grenvall C, Antfolk C, Bisgaard C Z and Laurell T 2014 Two-dimensional acoustic particle focusing enables sheathless chip Coulter counter with planar electrode configuration *Lab Chip* **14** 4629–37

[22] Manneberg O, Svennebring J, Hertz H M and Wiklund M 2008 Wedge transducer design for two-dimensional ultrasonic manipulation in a microfluidic chip *J. Micromech. Microeng.* **18** 095025

[23] Nordin M and Laurell T 2012 Two-hundredfold volume concentration of dilute cell and particle suspensions using chip integrated multistage acoustophoresis *Lab Chip* **12** 4610–6

[24] Settnes M and Bruus H 2012 Forces acting on a small particle in an acoustical field in a viscous fluid *Phys. Rev.* E **85** 016327

[25] Baroud C N, Gallaire F and Dangla R 2010 Dynamics of microfluidic droplets *Lab Chip* **10** 2032–45

[26] Kinsler L E 2000 *Fundamentals of Acoustics* 4th edn (New York: Wiley) p 548

[27] Manneberg O, Vanherberghen B, Onfelt B and Wiklund M 2009 Flow-free transport of cells in microchannels by frequency-modulated ultrasound *Lab Chip* **9** 833–7

[28] Iranmanesh I, Barnkob R, Bruus H and Wiklund M 2013 Tunable-angle wedge transducer for improved acoustophoretic control in a microfluidic chip *J. Micromech. Microeng.* **23** 105002

[29] Lenshof A, Evander M, Laurell T and Nilsson J 2012 Acoustofluidics 5: building microfluidic acoustic resonators *Lab Chip* **12** 684–95

[30] Baret J C 2012 Surfactants in droplet-based microfluidics *Lab Chip* **12** 422–33

[31] Schneider C A, Rasband W S and Eliceiri K W 2012 NIH image to ImageJ: 25 years of image analysis *Nat. Methods* **9** 671–5

[32] Muller P B, Barnkob R, Jensen M J H and Bruus H 2012 A numerical study of microparticle acoustophoresis driven by acoustic radiation forces and streaming-induced drag forces *Lab Chip* **12** 4617–27

[33] Bruus H 2008 *Theoretical Microfluidics* (*Oxford Master Series in Physics*) (Oxford: Oxford University Press) p 346

[34] Wiklund M 2012 Acoustofluidics 12: biocompatibility and cell viability in microfluidic acoustic resonators *Lab Chip* **12** 5283

[35] Barnkob R, Augustsson P, Laurell T and Bruus H 2012 Acoustic radiation- and streaming-induced microparticle velocities determined by microparticle image velocimetry in an ultrasound symmetry plane *Phys. Rev.* E **86** 056307

[36] Kinoshita H, Kaneda S, Fujii T and Oshima M 2007 Three-dimensional measurement and visualization of internal flow of a moving droplet using confocal micro-PIV *Lab Chip* **7** 338–46

[37] Ma S H, Sherwood J M, Huck W T S and Balabani S 2014 On the flow topology inside droplets moving in rectangular microchannels *Lab Chip* **14** 3611–20

[38] Hein M, Moskopp M and Seemann R 2015 Flow field induced particle accumulation inside droplets in rectangular channels *Lab Chip* **15** 2879–86